In-situ calibration of the single photoelectron charge response of the IceCube photomultipliers

IceCube author list to be inserted... E-mail: `analyses@icecube.wisc.edu`

ABSTRACT: This technical report outlines the in-situ calibration of the single photoelectron charge distributions for the Hamamatsu Photonics R7081-02 photomultipliers in the IceCube Neutrino Observatory. We discuss the single photoelectron extraction procedure, charge selection criteria, and report on various correlations between the shape of the charge distribution and hardware components. The time dependence of the charge distributions is also investigated.

KEYWORDS: IceCube, SPE Template, single photoelectron, PMT charge distribution.

Contents

1. Introduction

The IceCube Neutrino Observatory [1] is a cubic-kilometer sized array of 5,160 photomultiplier tubes (PMTs) buried in the Antarctic ice sheet designed to observe high energy neutrinos interacting with the ice [2]. As of 2011, the IceCube collaboration completed the installation of the main IceCube detector consisting of 78 cables, so called strings, and the low energy infill, DeepCore, consisting of a more densely arranged array of 8 strings. Each string in the detector contains 60 digital optical modules (DOMs), that house a single PMT each, as well as all required electronics. The DOMs extend from roughly 1450 m to 2450 m below the surface of the ice sheet and are spaced roughly 17 m apart in the IceCube detector and 7 m apart in the DeepCore detector.

    Each DOM consists of a 0.5" thick glass pressure vessel with a single down-facing 10" R7081-02 PMT from Hamamatsu Photonics [3]. The PMT is specified for wavelengths ranging from 300 nm to 650 nm, with peak quantum efficiency around 25% near 390 nm. Each PMT is coupled to the glass with optical gel and is surrounded by a wire mesh of μ-metal to reduce the effect of the

39 ambient Earth's magnetic field. The optical cut-off due to the glass is approximately 350 nm. The
40 R7081-02 has 10 dynode stages and is typically operated with a gain of 10^7 at 1300 V (a properly
41 amplified single photoelectron will create a $\approx 6\,\text{mV}$ peak voltage). The PMTs operate with the
42 anodes at high voltage, therefore the signal is AC coupled to the front-end amplifiers. There are
43 two versions of AC coupling in the detector both of which use custom designed bifilar-wound 1:1
44 toroidal transformers (the DOM specific AC coupling methods, new and old toroids, are shown in
45 the left side of Fig. 1).

46   IceCube has also deployed roughly 400 Hamamatsu R7081-02MOD DOMs [4], which, having
47 a peak quantum efficiency of 34% near 390 nm (36% higher efficiency than the standard DOMs),
48 are classified as high-quantum efficiency (HQE) DOMs. These DOMs are primarily located in
49 DeepCore, however there are a few located on string 36 and 43 as well, as shown in the center of
50 Fig. 1. Further information on the detector instrumentation can be found in Ref. [5,6].
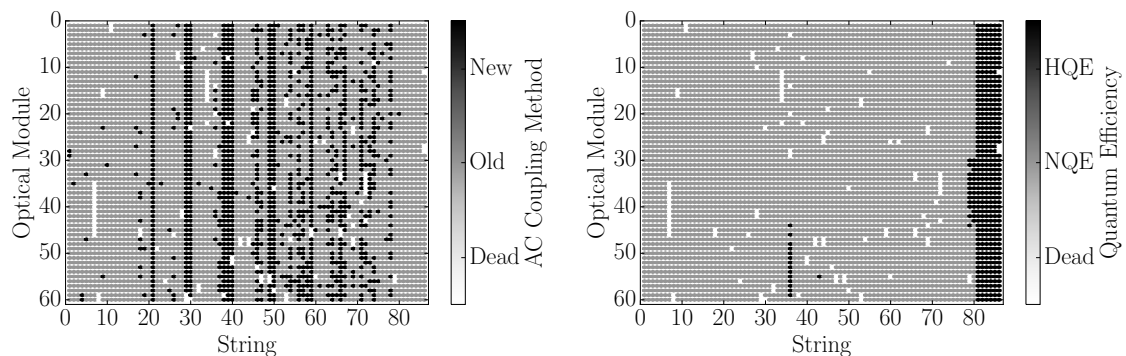
Figure 1. Left: The method of AC coupling, new toroids and old toroids. Middle: Mapping showing the HQE DOMs and standard DOMs. These figures also show the location of the dead DOMs in white.

51   The largest contribution to the IceCube trigger rate comes from down-going muons produced
52 in cosmic ray induced showers [7]. Cosmic ray muons stopping in the detector cause the individ-
53 ual DOM launch rate to decrease at lower depths. Further, during the formation of this ice sheet,
54 there have been several periods of colder climate (stadials) that have caused vastly different optical
55 properties in the ice at different depths. The optical properties also affect the DOM launch rate,
56 in particular, the "dust layer" from roughly 2100 to 2200 m (optical modules 32-38 in the IceCube
57 detector) below the surface is a region in the ice with a relatively large scattering and absorption co-
58 efficient. These factors can cause the DOM trigger rates to vary by nearly a factor of 10 depending
59 on the depth in the detector.

60   IceCube relies on two observables per DOM to reconstruct events: the total number of detected
61 photons (referred to as *charge*, after the PMT dynode stage) and their timing distribution. This
62 technical report is concerned with accurately determining how the DOMs collect charge in order to
63 improve calibration and the description of the detector in the Monte Carlo simulation. It describes
64 the procedure used to determine the PMTs gain characteristics as seen in the single photoelectron
65 charge distributions (SPE templates) using in-situ data from the IceCube and DeepCore detectors.
66 This was recently made possible by reducing the multi-PE contamination using a specially designed
67 pulse selection, and developing a method to account for the remaining multi-PE contamination
68 when fitting for the single photoelectron distribution.

In using in-situ data to measure the charge distributions, we accurately represent the individual PMT response as a function of time, environmental conditions, software version, hardware differences, and sample photons uniformly over the surface of the photocathode. This is beneficial since it also allows us to inspect the stability and long term behavior of the individual DOMs, verify previous calibration, and correlate features and environment to DOM behavior.

1.1 Single photoelectron charge distributions

In an idealistic scenario, a single photon produces a single photoelectron, which is then amplified by a known amount and the measured charge corresponds to 1PE. However, there are many physical processes which create structure in the measured charge distributions. For example:

- **Statistical fluctuation due to cascade multiplication** [8]. At every stage of dynode amplification, there is a stochastic spread in the number of emitted electrons that make it to the next dynode. This in turn causes a spread in the measured charge after the gain stage of the PMT.

- **Photoelectron trajectory**. Some electrons may deviate from the favorable trajectory, reducing the effective multiplication. This can occur at all dynodes, however, it has the largest effect on the multiplication at the first photoelectron [9]. The trajectory of the photoelectron striking the first dynode will depend on many things, include where on the photocathode it was emitted, the uniformity of the electric field, the size and shape of the dynode [8], and the magnetic field [10, 11].

- **Late or delayed pulses**. A photoelectron can (in-)elastically scatter off the first dynode. The scattered electron can then be re-accelerated to the dynode, and creates a second pulse that is also lower in charge. The difference in time between the initial pulse and the re-accelerated pulse in the R7081-02 was previously measured to be up to 70 ns [6, 12]. Collecting either the initial pulse or the late pulse will result in the charge falling into the low-PE charge region.

- **After-pulses**. As the electrons gain energy in the cascade multiplication chain, they can ionize residual gas between dynodes, which then can itself accelerate towards the dynodes. For the IceCube PMTs, the timescale for after-pulses was measured to occur roughly 0.3 to 12 μs after the initial pulse [6]. This populates the low-PE charge region since some of the energy of the electron avalanche goes into the ionization of the residual gas.

- **Pre-pulses**. If the incident photon passes through the photocathode without interaction and strikes one of the dynodes, it can eject an electron thus causing the measured charge to be lower. For the IceCube PMTs, the pre-pulses were found to arrive approximately 30 ns before the signal from other photoelectrons from the photocathode [6]. Further detail is available in Ref. [13].

- **Multi-PE contamination**. When multiple photoelectrons arrive at the dynodes within several nanoseconds of each other, they can be reconstructed by the software as a single, multi-PE pulse.

The previous IceCube charge distribution (known as the TA0003 distribution) modeled the above effects as the sum of an exponential plus a Gaussian, where the exponential represented poorly amplified pulses, and the Gaussian represented the spread in properly amplified pulses. Subsequent measurements illustrated that when measuring charge below the discriminator, the description of the shape was improved with the addition of a second, steeply falling exponential (Exp_1) to account for the low-PE charge region:

$$f(q) = E_1 e^{-q/w_1} + E_2 e^{-q/w_2} + N e^{-0.5 \frac{(q-\mu)^2}{\sigma^2}}. \tag{1.1}$$

This is the SPE template functional form that is used in this report. IceCube calibrates the gain on the individual DOMs during the start of each season to ensure that the Gaussian mean component, μ, of the SPE template (which defines 1PE) equals 10^7 electrons.

The shape of $f(q)$ is finite down to 0 PE, however due to the discrete nature of the ADC and the fluctuations about the baseline, some assumption on the shape must be inferred in the low-PE charge region.

The multi-PE contamination to the charge distribution is assumed to be the convolution of the SPE distribution multiple times [14]. That is, the two-PE distribution is assumed to the be SPE distribution convolved with itself. A python based piece of software called the "convolutional fitter" is used to determine the components of Eq. 1.1.

1.2 IceCube datasets and software definitions

An induced signal in the PMT will pass through the AC coupling toroid located on the base of the PMT, then be compared to a discriminator threshold set to 0.25 PE. The crossing of the discriminator threshold begins a "DOM launch" and the waveforms are recorded with a high-speed 10-bit waveform digitizer (Analog Transient Waveform Digitizer, ATWD).

For each triggered window, the ATWD samples 128 times at 300 MHz. In order to be able to trigger the ATWD and record baseline data prior to the pulse, the analog input from the PMT is sent through a delay board, which delays the signal by approximately 75 ns.

After waveform digitization, there is a correction applied to remove any DC baseline offset and correct for the signal droop introduced by the AC coupling. The waveform is then passed through pulse extraction software (WaveDeform [15]) to de-convolute the waveform into a so-called *pulse series* of scaled SPE pulses, each with a time and charge in terms of SPE. WaveDeform also attempts to takes into account the SPE waveform shape difference between the new and old versions of AC coupling.

The pulse series used in this analysis come from two datasets:

1. The **MinBias dataset** records the full waveform of randomly selected events, at a rate that corresponds on average to 1/1000 events. This dataset is used for determining the individual DOM charge distributions.

2. The **BeaconLaunch dataset** is a forced-trigger (not triggered by the discriminator) filter that is typically used to monitor the individual DOM baseline. It therefore also includes the full window waveform readout. Since this dataset is forced-triggered, the majority of these waveforms represent baseline fluctuations, however there will be the occasional coincidental

144   pulse that makes it into the readout window. This dataset will be used to examine the noise
145   contribution to the charge distributions.

146   This analysis uses the full MinBias and BeaconLaunch datasets from IceCube season 2011 to
147   2016. Seasons in IceCube typically start in June of the labeled year and end roughly one year later.

2. Single photoelectron pulse selection

149   The pulse selection is the method used to extract candidate, unbiased, single photoelectrons from
150   data. An illustrative digram of the pulse selection is shown in the left side of Fig. 2, and a descrip-
151   tion of the procedure is detailed below.
152   In order to trigger a DOM, the ATWD voltage must exceed the discriminator threshold. Since
153   the SPE templates must be defined to 0PE, the aim is to characterize the measured charge distri-
154   bution to as low-PE charge as possible. This means that the pulses subject to the discriminator
155   must be removed. This is accomplished by ignoring pulses that arrive within the first 100 ns of
156   the time window. The triggering pulse is removed by rejecting the first 100 ns of the time window.
157   Restrictions are put on the allowed waveforms as well, such as ensuring that the trigger pulse does
158   not exceed 10 mV (to reduce droop due to the AC coupling) as well as a global constraint that the
159   time window cannot contain any pulses that exceeds 20 mV. Pulses that arrive over 400 ns after the
160   trigger may be partially attributed to after pulses, therefore, we do not accept pulses that arrive late
161   in the time window (over 375 ns after the trigger). Finally, to avoid including late-pulses from the
162   trigger, we also enforce that the pulse of interest (POI) arrives later than 100 ns after the trigger.
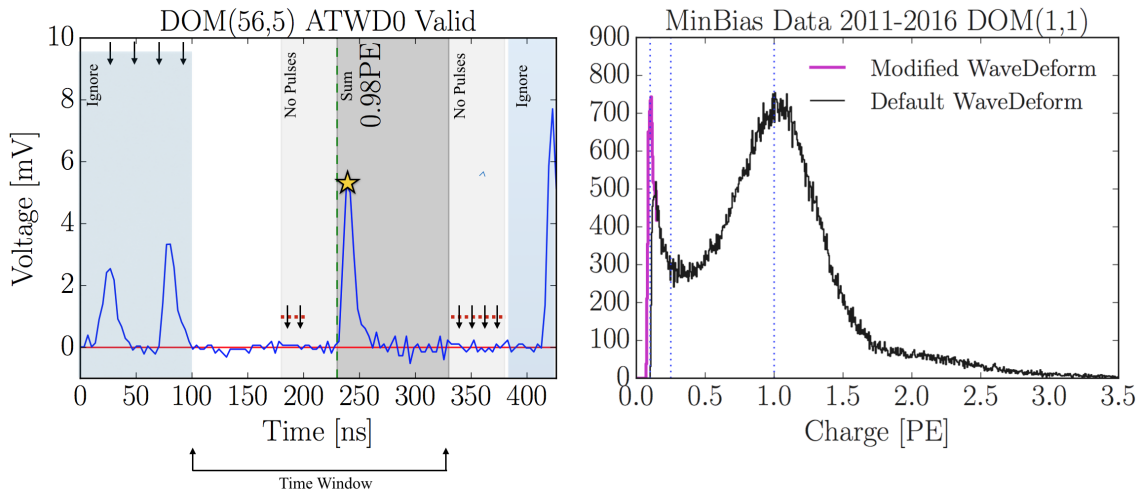
Figure 2. Left: The pulse selection criteria for a selecting a high purity and unbiased sample of single photoelectrons. Right: the collected charges from string 1, optical module 1 (DOM 1,1) from the MinBias data collected from 2011 to 2016 using the pulse selection. The discriminator threshold at 0.25PE is shown as a dotted vertical line (as well as lines at 0.10PE and 1PE). The black histogram is the charge distribution using the non-modified WaveDeform, whereas the purple low-PE component is measured using a modified version of WaveDeform described in Sec. 3.

If a pulse is reconstructed between 100 and 375 ns after the time window is opened, it is accepted as a candidate photoelectron and several checks are performed to ensure the stability of the waveform. The first check is to ensure that the waveform is at the baseline just prior to the rising edge of the POI. This is accomplished by ensuring that the waveform does not exceed 1 mV, 50 to 20 ns prior to the POI. We also ensure the waveform returns to the baseline by checking that no ADC measurement exceeds 1 mV, 100 to 150 ns after the POI. If both these criteria are met, we sum the reconstructed charges from the pulse time (given by WaveDeform) to +100 ns. The purpose of this summation is to reassemble charges that may have accidentally been split by WaveDeform and to reassemble late-pulses. This also means that we will occasionally be accepting multi-PE events.

The pulse selection provides a relatively pure sample of single photoelectrons (as shown in the black histogram on the right side of Fig. 2. It rejects after-pulses, reassembles late pulses, avoids the discriminator threshold, reduces the effect of droop/sag, gives sufficient statistics to perform a season-to-season measurement, and has a minimal amount of multi-PE contamination.

The right side of Fig. 2 also shows that there is a second threshold (in the black histogram) at approximately 0.15PE. This is a software defined threshold that comes from WaveDeform not attempting to deconvolve charges smaller than a certain size. This threshold is not sharply defined, therefore it is difficult to draw conclusions about the low-PE tail without further investigation. Determining the shape of the low-PE charge region involves modifying WaveDeform.

3. Characterizing the low-PE charge region

IceCube has performed several lab measurements using the IceCube PMTs with in-time laser pulses that have shown a steeply falling low-PE tail below the discriminator threshold. This is in agreement with the in-ice measurements performed by this analysis. In order to reconstruct smaller charges, Wavedeform was minimally modified to access smaller charges in the pulse selection. The modifications brought the reconstruction threshold down below 0.10PE, as shown in the purple histogram of the right side of Fig. 2.

In the context of monitoring the waveforms, noise will be defined as ADC fluctuations or ringing arising from the pedestal. As the modifications to WaveDeform lower the measured charge threshold, the amount of reconstructed noise increases. To quantify the amount of noise introduced into the charge distribution, the BeaconLaunch dataset is used.

The pulse selection described in Sec. 2, was run on the full BeaconLaunch dataset before and after the modifications to WaveDeform, this is shown in the light and dark blue histogram of Fig. 3. The BeaconLaunch data in this figure has been scaled by a factor of 163 such that the total livetime of the BeaconLaunch dataset was that of the MinBias dataset. In the region below 0.10PE, we find that the noise contributes less than 1/10th of the total charge.

4. Extracting the SPE templates

4.1 Fitting procedure

Pulses that fall below the WaveDeform threshold and are not reconstructed contribute to an effective efficiency of the individual DOM. This analysis assumes the same shape of the steeply
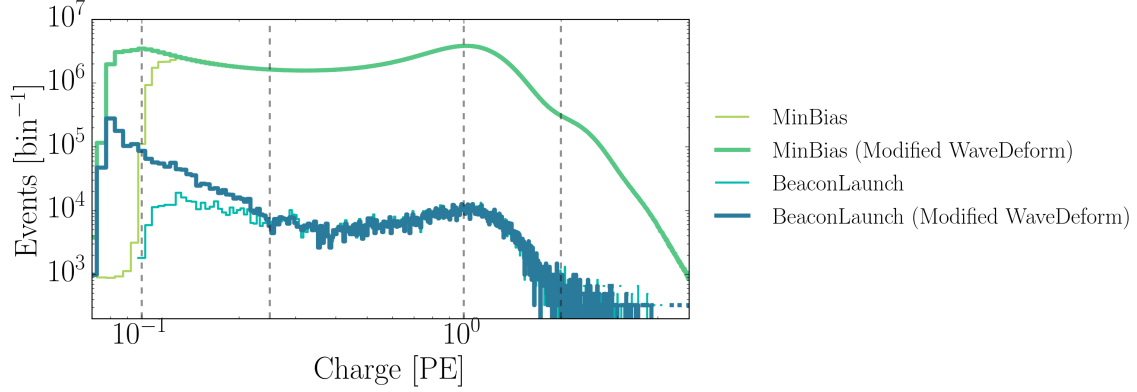
Figure 3. The cumulative charge distributions of all DOMs for the MinBias and BeaconLaunch datasets, for both the modified and non-modified version of WaveDeform. The BeaconLaunch datasets have been scaled such that their livetime matches that of the MinBias dataset. Vertical dotted lines are shown at 0.10PE, 0.25PE, 1PE and 2PE.

falling exponential component (Exp_1) for all DOMs in the detector to avoid large fluctuations in the individual DOM efficiencies. The shape of Exp_1 is determined by fitting the cumulative charge distribution for all DOMs, for all seasons and uses the modified WaveDeform datasets.

The fit assumes that there is a negligible three-PE contribution, which is evident both by the lack of statistics in the 3PE region, as well as the significant scale difference between the 1PE and 2PE region).

The second exponential (Exp_2, components E_2 and w_2 of Eq. 1.1), represents poorly amplified photoelectrons and therefore we do not allow it to extend beyond the high charge region of the Gaussian component. In particular, we include a constraint on the the parameter w_2 to ensure that it falls off with the Gaussian component:

$$w_2 < \frac{\mu + 2\sigma}{4 - \text{Ln}(N/E_1)} \tag{4.1}$$

This equation was found by setting the Exp_2 to be $1/e^2$ that of the Gaussian component at two sigma.

To avoid the Gaussian component extending below the 0 PE, a constraint on the Gaussian width, σ of Eq. 1.1, is set to be:

$$\sigma < \frac{0.5\mu^2}{\text{Ln}(100)} \tag{4.2}$$

This constraint enforces that the Gaussian component at 0PE is less than 1% the amplitude of the Gaussian.

The convolutional fitter is used with the constraints (Eq. **??**) to extract the fit components to the measured charge distributions. First, it is used to determine the shape of Exp_1 using the cumulative charge distributions of all the DOMs summed together, with the modified BeaconLaunch dataset subtracted from the modified MinBias dataset. Then, the shape of Exp_1 is inserted into all subsequent fits using the non-modified MinBias datasets.

4.2 SPE template fit results

Using the background subtracted modified WaveDeform dataset, the steeply falling exponential component was determined by fitting from 0.1PE to 3.5PE to be $E_1 = 6.9 \pm 1.5$ and $w_1 = 0.032 \pm 0.002$PE. The shape of the steeply falling exponential is then used to describe the low-PE charge region for all subsequent non-modified WaveDeform fits. These fits are performed for each individual DOM, separately for each IceCube season (IC86.2011 to IC86.2016), and for the individual DOM cumulative fit where all the seasons are summed together (labeled as "AVG"). Failed fits (dead DOMs, DOMs with known problems, or DOMs that fail any one of several validity checks on the goodness of fit) are not included in this analysis, however, in simulation they are given the average SPE template shape.

The fit range is selected to be between 0.2PE and 3.5PE. An example fit is shown in Fig. 4 for the cumulative charge distribution for string 1, optical module 1 (DOM (1,1)). The collected charge is shown in the black histogram, while the convolutional fit is shown as the black line. The extracted SPE template for this DOM is shown in red. The fit components, in green, show the steeply falling exponential at low charge, the Gaussian and second exponential, and the 2PE contribution (the multi-PE contamination).
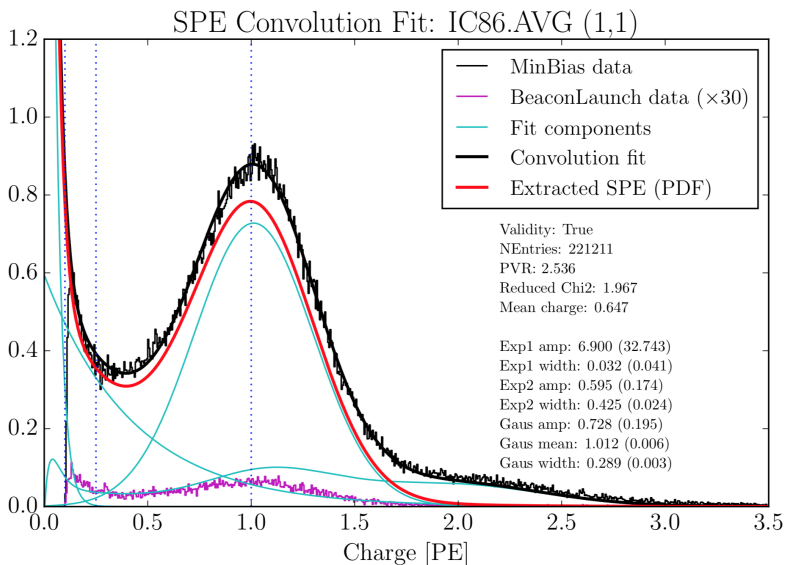
Figure 4. An example fit result for DOM (1,1) using the non-modified WaveDeform and data from all seasons. The result from the convolutional fitter is shown in black and the components of the fit are shown in green. The extracted SPE template is shown in red. The purple histogram is the full detector (all DOMs summed together) non-modified BeaconLaunch dataset, scaled to the livetime of the MinBias data and further multiplied by a factor of 30 in order to be visible.

The mean value and 1σ spread of the fit parameters, excluding Exp_1 and the Gaussian mean (since it is calibrated to be unity), for the IceCube (DeepCore) detector is shown in Table 1 (Table 2). The overall shape of the distribution, the mean value of the fit parameters, and the spread were found to stable over the six seasons of analyzed data.

The individual DOM SPE templates were then examined between IceCube seasons. For every DOM, the change over time of each fit parameter was calculated.

IceCube	Exp$_2$ Amplitude	Exp$_2$ Width	Gaus. Amplitude	Gaus. Width
IC86.2011	0.552 ± 0.070	0.419 ± 0.036	0.721 ± 0.057	0.305 ± 0.019
IC86.2012	0.553 ± 0.069	0.418 ± 0.036	0.722 ± 0.057	0.305 ± 0.020
IC86.2013	0.555 ± 0.068	0.417 ± 0.036	0.721 ± 0.056	0.305 ± 0.020
IC86.2014	0.553 ± 0.068	0.419 ± 0.035	0.720 ± 0.056	0.306 ± 0.019
IC86.2015	0.554 ± 0.070	0.418 ± 0.038	0.722 ± 0.057	0.305 ± 0.020
IC86.2016	0.554 ± 0.069	0.418 ± 0.036	0.721 ± 0.057	0.305 ± 0.020

Table 1. The average fit value and 1σ spread for the IceCube detector.

DeepCore	Exp$_2$ Amplitude	Exp$_2$ Width	Gaus. Amplitude	Gaus. Width
IC86.2011	0.604 ± 0.067	0.417 ± 0.029	0.678 ± 0.040	0.312 ± 0.016
IC86.2012	0.606 ± 0.070	0.416 ± 0.030	0.679 ± 0.040	0.312 ± 0.015
IC86.2013	0.610 ± 0.067	0.413 ± 0.029	0.678 ± 0.041	0.311 ± 0.016
IC86.2014	0.609 ± 0.066	0.414 ± 0.031	0.677 ± 0.040	0.312 ± 0.015
IC86.2015	0.607 ± 0.063	0.417 ± 0.029	0.680 ± 0.041	0.311 ± 0.016
IC86.2016	0.610 ± 0.065	0.415 ± 0.030	0.679 ± 0.040	0.311 ± 0.016

Table 2. The average fit value and 1σ spread for the DeepCore detector.

Fig. 5 shows the change in a given fit parameter (represented in percentage deviation from the mean value), per year, of each DOM in both the IceCube (left) and DeepCore (right) detectors. All the fit parameters are found to deviate less than 0.1% per year in both detectors, which is in agreement with the stability checks performed in Ref. [5].
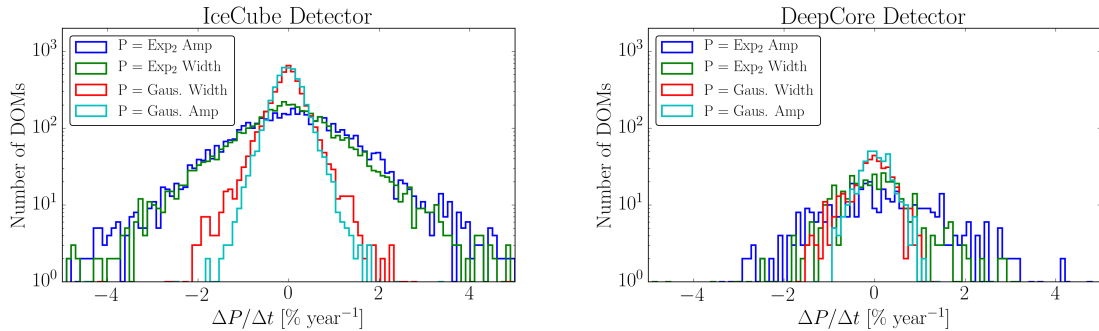
Figure 5. The change in individual DOM fitted parameters over time (left: IceCube, Right: DeepCore). The change in the fit value is represented in percentage deviation from the mean fit parameter value.

5. Discussion

5.1 Correlations between fit parameters and DOM hardware differences

As noted in Sec. 1, there are two hardware differences implemented in the deployment of the DOMs: subset of HQE DOMs and the method used for AC coupling the PMT anode to the front-

end amplifiers. Correlations between the different hardware configurations were examined for correlations with the SPE template fit components.

The HQE DOMs were found to have a larger Exp_2 component (9.2% lower w_2 component, and a 17.2% higher E_2, described in terms of Eq.1.1) than the standard DOMs in IceCube. Consequently, the HQE DOMs have an 11.6% lower peak-to-valley ratio and a 3.7% lower mean charge. These distributions are shown in Fig. 6.
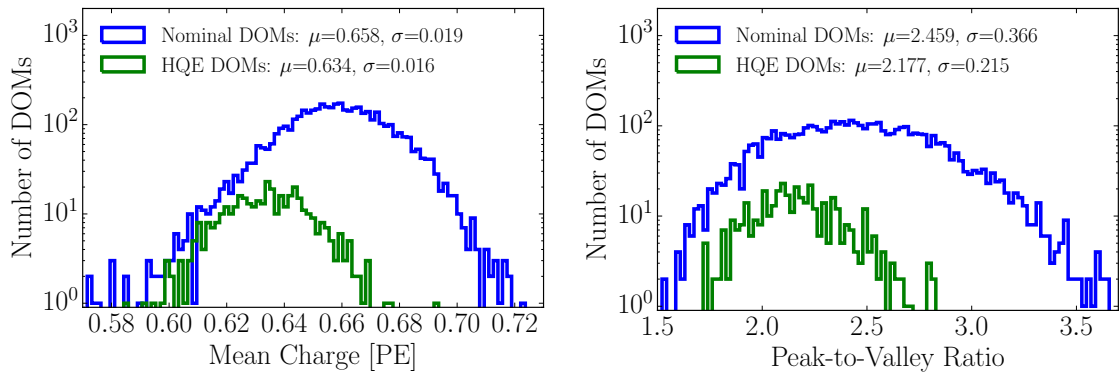
Figure 6. Comparison between the R7081-02MOD HQE DOMs and standard R7081-02 DOMs. Left: The mean charge of the individual DOM SPE templates. Right: The Peak-to-Valley ratio for the two subsets of quantum efficiencies.

The DOMs with the old method of AC coupling were found to have a 7.2% narrower Gaussian width and an 8.0% larger Gaussian amplitude (σ and N in Eq. 1.1) . The exponential component, however, was found to be within 0.9% of the average DOMs. Although the old toroid DOMs were deployed into ice earlier than the new toroid DOMs, the difference above is still noted when examining individual deployment years, therefore the shape differences are not attributed to the change in the DOM behavior over time. However, the DOMs with the old toroids were the first DOMs to be manufactured by Hamamatsu, therefore, this difference may also be attributed to a change in the production procedure rather than the actual AC coupling method.
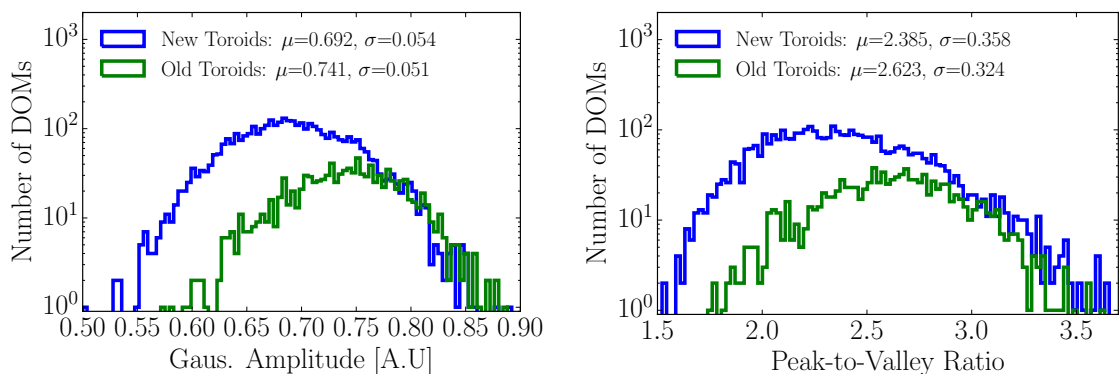
Figure 7. Comparison between the AC coupling method used on the DOMs. Left: The Gaussian amplitude fit component, N. Right: The Peak-to-Valley ratio for the subset of DOMs with different AC coupling.

6. Conclusion

This report outlines the procedure used for collecting a relatively pure sample of single photo electronics from in-ice IceCube data. Multi-PE contamination was removed using the assumption that the MPE contamination is the convolution of the SPE distribution mutliple times. The correlations between the extracted shape of the SPE templates and hardware specific differences in the DOMs was investigated. Sub-percent level seasonal variations were observed, in agreement with Ref. [5]. Individual DOM seasonal variations were found to be sub 0.1% per year. The HQE DOMs located in the IceCube and DeepCore detectors, were found to have a distinguishable Exp_2 component from the standard DOMs. Similarly, DOMs with different AC coupling were also found to have a distinguishable shape difference, however, this could have been due to the manufacturing process of the DOMs rather than the method of AC coupling.

References

[1] J. Ahrens *et al.*, "Icecube preliminary design document," *URL http://www. icecube. wisc. edu/science/publications/pdd*, 2001.

[2] I. Collaboration *et al.*, "Evidence for high-energy extraterrestrial neutrinos at the icecube detector," *Science*, vol. 342, no. 6161, p. 1242856, 2013.

[3] Hamamatsu, "Datasheet."

[4] R. Abbasi, Y. Abdou, T. Abu-Zayyad, M. Ackermann, J. Adams, J. Aguilar, M. Ahlers, M. Allen, D. Altmann, K. Andeen, *et al.*, "The design and performance of icecube deepcore," *Astroparticle physics*, vol. 35, no. 10, pp. 615–624, 2012.

[5] M. Aartsen *et al.*, "The icecube neutrino observatory: Instrumentation and online systems, jinst 12 (03)(2017) p03012," *arXiv preprint arXiv:1612.05093*, pp. 1748–0221.

[6] R. Abbasi, Y. Abdou, T. Abu-Zayyad, J. Adams, J. Aguilar, M. Ahlers, K. Andeen, J. Auffenberg, X. Bai, M. Baker, *et al.*, "Calibration and characterization of the icecube photomultiplier tube," *Nuclear Instruments and Methods in Physics Research Section A: Accelerators, Spectrometers, Detectors and Associated Equipment*, vol. 618, no. 1-3, pp. 139–152, 2010.

[7] M. Aartsen, K. Abraham, M. Ackermann, J. Adams, J. Aguilar, M. Ahlers, M. Ahrens, D. Altmann, T. Anderson, M. Archinger, *et al.*, "Characterization of the atmospheric muon flux in icecube," *Astroparticle physics*, vol. 78, pp. 1–27, 2016.

[8] Hamamatsu, "Basics and applications," Third Edition.

[9] Hamamatsu, "Handbook, chapter 4."

[10] J. Brack, B. Delgado, J. Dhooghe, J. Felde, B. Gookin, S. Grullon, J. Klein, R. Knapik, A. LaTorre, S. Seibert, *et al.*, "Characterization of the hamamatsu r11780 12 in. photomultiplier tube," *Nuclear Instruments and Methods in Physics Research Section A: Accelerators, Spectrometers, Detectors and Associated Equipment*, vol. 712, pp. 162–173, 2013.

[11] E. Calvo, M. Cerrada, C. Fernández-Bedoya, I. Gil-Botella, C. Palomares, I. Rodríguez, F. Toral, and A. Verdugo, "Characterization of large-area photomultipliers under low magnetic fields: Design and performance of the magnetic shielding for the double chooz neutrino experiment," *Nuclear Instruments and Methods in Physics Research Section A: Accelerators, Spectrometers, Detectors and Associated Equipment*, vol. 621, no. 1-3, pp. 222–230, 2010.

[12] F. Kaether and C. Langbrandtner, "Transit time and charge correlations of single photoelectron events in r7081 photomultiplier tubes," *Journal of Instrumentation*, vol. 7, no. 09, p. P09002, 2012.

[13] B. Herold, O. Kalekin, *et al.*, "Pmt characterisation for the km3net project," *Nuclear Instruments and Methods in Physics Research Section A: Accelerators, Spectrometers, Detectors and Associated Equipment*, vol. 626, pp. S151–S153, 2011.

[14] R. Dossi, A. Ianni, G. Ranucci, and O. J. Smirnov, "Methods for precise photoelectron counting with photomultipliers," *Nuclear Instruments and Methods in Physics Research Section A: Accelerators, Spectrometers, Detectors and Associated Equipment*, vol. 451, no. 3, pp. 623–637, 2000.

[15] M. Aartsen *et al.*, "Energy reconstruction methods in the icecube neutrino telescope, jinst 9 (2014) p03009," *arXiv preprint arXiv:1311.4767*, pp. 1748–0221.

7. Appendix

7.1 Quantifying the effect of using SPE templates

Changing the assumed gain response in simulation, as deduced from data, has different implications depending on the typical illumination level as present in different analysis. These differences are outlined in the following.

The PMT response is described by a combination of a "bare" efficiency, η_0, and a normalized charge response function, $f(q)$. The bare efficiency represents the fraction of arriving photons that result in any non-zero charge response, including those well below the discriminator threshold. The normalization condition is:

$$\int_0^{\inf} f(q)dq = 1. \tag{7.1}$$

Generally, $f(q)$ and η_0 have to be adjusted together to maintain agreement with a quantity known from lab or in-ice measurements, such as the predicted number of pulses above threshold for a dim source.

7.1.1 Dim source measurements

Where light levels are low enough, sub-discriminator pulses do not contribute any observed charge because they do not satisfy the trigger threshold and the probability of two photons arriving together is negligible. Given some independent way of knowing the number of arriving photons, a lab or in-ice measurement determines the trigger fraction above threshold $\eta_{0.25}$ and/or the average charge over threshold $Q_{0.25}$, either of which can be used to constrain the model as follows:

$$\eta_{0.25} = \eta_0 \int_{0.25q_{pk}}^{\inf} f(q)dq \tag{7.2}$$

$$Q_{0.25} = \eta_0 \int_{0.25q_{pk}}^{\inf} qf(q)dq \tag{7.3}$$

Here, the discriminator threshold is assumed to be 0.25 times the peak position q_{pk}. It is also useful to scale observed charges by q_{pk}, since we set each PMT gain by such a reference, and then a measurement constraint would be stated in terms of $Q_{0.25}/q_{pk}$.

7.1.2 Semi-bright source measurements

Once the ATWD window is open, subsequent pulses are not limited by the discriminator threshold, however, WaveDeform introduces a software threshold at 0.1PE (described at the end of Section 2). The average charge of an individual pulse that arrive within the time window is therefore:

$$Q_{0.10} = \eta_0 \int_{0.10q_{pk}}^{\inf} qf(q)dq \tag{7.4}$$

7.1.3 Bright source measurements

For light levels that are large, the trigger is satisfied regardless of the response to individual photons, and the total charge per arriving photon therefore includes contributions below both the discriminator and the WaveDeform thresholds:

$$Q_0 = \eta_0 \int_0^{\inf} q f(q) dq \qquad (7.5)$$

As such the total charge is directly proprotianal to the average charge of the SPE template, having a strong dependence on the steeply falling exponential.

7.1.4 Model comparison

When the charge distribution model is changed in a way that preserves agreement with the measured $\eta_{0.25}$ or $Q_{0.25}/q_{pk}$, i.e. η_0 is adjusted properly for changes in $f(q)$, the physical effect can be summarized by the change in the bright-to-dim ratios $Q_0/Q_{0.25}$, and $Q_0/Q_{0.10}$. Conveniently, these ratios depend only on the shape of $f(q)$. Table 3 compares these ratios in terms of the previous charge distribution (TA0003) and the SPE templates described here.

Model	Detector	$Q_0/Q_{0.25}$	$Q_0/Q_{0.10}$	$\eta_{0.25}/Q_{0.25}$
TA0003	IceCube and DeepCore	1.017	1.003	0.969
SPE Templates	IceCube	1.031±0.003	1.013±0.001	0.971±0.006
SPE Templates	DeepCore	1.034±0.002	1.014±0.001	0.965±0.006

Table 3. The distribution in bright-to-dim ratios for the previous charge distribution (TA0003) and the individual DOM SPE templates for the IceCube and DeepCore detector.
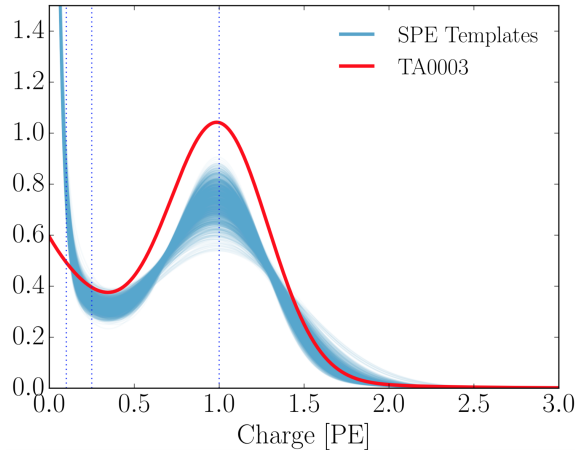
Figure 8. The normalized charge distributions. The TA0003 distribution is shown in red, while the cumulative SPE templates for DOMs in both IceCube and DeepCore are shown in Blue.

Table 3, shows percent-level differences in the physically observable bright-to-dim ratios. Fig. 8, shows the shape difference between the TA0003 distribution and all the SPE templates

measured in this report. The shape difference is attributed to a better control of the low charge region, the difference in functional form (described in Section 1.1), as well as the fact that the SPE templates sample uniformly over the entire photocathode at random incident angles.